

# An adaptive phase recovery method for 4D phase-contrast MRI

Rizwan Ahmad<sup>1</sup>, Ning Jin<sup>2</sup>, Yu Ding<sup>3</sup>, and Orlando P Simonetti<sup>3</sup>

<sup>1</sup>Electrical Engineering, The Ohio State University, Columbus, OH, United States, <sup>2</sup>Siemens Healthcare, Columbus, OH, United States, <sup>3</sup>Internal Medicine, The Ohio State University, Columbus, OH, United States

**Target Audience:** Researchers and practitioners interested in developing methods to improve accuracy of blood flow measurement using PC-MRI.

**Purpose:** Balanced four-point encoding (BFPE)<sup>1</sup> is a commonly employed encoding strategy for 4D PC-MRI. Recently, we proposed a method, called direct reconstruction (DiR), which overcomes some of the limitations of standard sliding window approach. DiR is based on solving an underdetermined set of equations via regularized least-squares. Being a linear method, DiR treats all velocity components equally, i.e., it assigns equal bandwidth to each component even when the true frequency contents of the components are widely different from each other. Therefore, in DiR, the assigned bandwidth (BW<sub>a</sub>) for each component cannot exceed 1/4<sup>th</sup> the total bandwidth (BW<sub>t</sub>), which is determined by the temporal sampling frequency. To overcome this limitation, here, we provide an adaptive formulation of DiR, called adaptive DiR (DiRa), where the BW<sub>a</sub> of each velocity component is adapted based on a current estimate of its temporal frequency contents. This setup allows components with more signal energy in the high-pass region to have higher BW<sub>a</sub>, leading to improved temporal resolution and reduced artifacts.

**Methods:** The recently proposed DiR method can be mathematically written as:  $\hat{\phi}_{DiR} = (B^T B + \lambda R^T R)^{-1} B^T \theta$  (Eq. 1), where  $\theta$  represents all  $N$  noisy measurements across time,  $B$  is a  $N \times 4N$  underdetermined matrix that represents the forward model,  $R$  is a high-pass filter that provides stability to the underdetermined system of equations,  $\lambda$  controls the extent of regularization, and  $\hat{\phi}_{DiR}$  is a  $4N \times 1$  vector that represents an estimate of the true unknown phase  $\phi$ . In contrast, the proposed DiRa is formulated as

$$\hat{\phi}_{DiRa} = \underset{\lambda_b, \lambda_x, \lambda_y, \lambda_z, \phi}{\operatorname{argmin}} \|\theta - B\phi\|_2^2 + \lambda_b \|R_b \phi\|_2^2 + \lambda_x \|R_x \phi\|_2^2 + \lambda_y \|R_y \phi\|_2^2 + \lambda_z \|R_z \phi\|_2^2$$

Here,  $\lambda_b, \lambda_x, \lambda_y,$  and  $\lambda_z$  control the extent of regularization for the background,  $x,$   $y,$  and  $z$  components of the unknown phase (velocity), respectively, and the linear operator  $R_i$  indicates that the regularization is acting only on the “\*” component. We selected matrix  $R$  to be a finite difference approximation to the second derivative with respect to time. To solve for  $\hat{\phi}_{DiRa}$  in Eq. 2, we adopted an alternating minimization scheme: (i) solve for  $\phi$  for given values of  $\lambda_b, \lambda_x, \lambda_y, \lambda_z$  (closed form), (ii) solve for  $\lambda_b, \lambda_x, \lambda_y, \lambda_z$  for a given value of  $\phi$  (closed form), and (iii) iterate over the last two step until convergence is reached. Once the phase is estimated, it is scaled with appropriate values of velocity encoding gradients to yield estimated velocity profiles. Note, both DiR and DiRa operate on reconstructed phase images on pixel-by-pixel basis, and the process (Eq. 1 for DiR and Eq. 2 for DiRa) is repeated for all pixels.

**Results:** Four components of velocity ( $v_x, v_y, v_z,$  and  $v_b$ ) were simulated in Matlab using Hann functions. The BFPE data were generated from the simulated velocity profiles. A total of 256 trial runs were considered with different realizations of noise. Also, in each trial run, the widths of the four Hann functions were selected randomly, allowing the components to have different frequency contents. The results from one trial run are shown in Figure 1. Peak velocity error (computed as a percentage of the true peak velocity) is shown in Figure 2.

Experimental data were collected from a pulsatile homebuilt phantom using a 1.5 T clinical scanner (Siemens Medical Solutions, Germany) using body matrix receive coils. Six identical datasets were collected using an EPI-PC sequence with BFPE, echo-train-length=7, matrix size=128x96, TE=13.2 ms, TR=23.5 ms, lines/segment=7, number of frames=32, parallel acceleration factor=2. For reference standard, GRE-PC sequence was used with referenced four-point encoding, TE = 3.28 ms, TR=5.9 ms, lines per segment=1, number of frames=32, and parallel acceleration factor=2. For both EPI-PC and GRE-PC datasets, TGRAPPA<sup>3</sup> was used for frame-by-frame image reconstruction. The DiR and DiRa methods were then applied on the resulting phase images to reconstruct velocity profiles at each pixel from the EPI-PC data. See results in Figure 3.

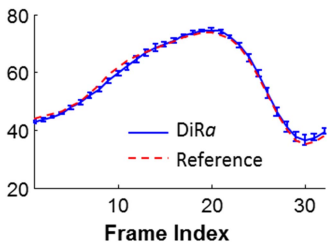


**Figure 3:** Peak velocity profiles from the pulsatile phantom data. Each entry in the profile represents the maximum (across all pixels) velocity magnitude in a frame. For DiRa,  $n=6$ .

**Discussion:** Each velocity component in DiR is assigned 1/4<sup>th</sup> of BW<sub>t</sub>. In practice, different components may have different frequency contents. For example, if the encoding direction is aligned with the flow direction at a given pixel, the signal for that pixel will primarily reside in one of the three spatial components. In this case, it is not reasonable to waste 1/4<sup>th</sup> of BW<sub>t</sub> on components that have minimum or no signal energy. Also, background phase may vary slowly over time, i.e., has a small value of  $\|R_b \phi\|_2^2$ , and may require less than 1/4<sup>th</sup> of BW<sub>t</sub> for high-fidelity representation. The proposed adaptive method, DiRa, by independently adjusting the regularization weight on each component, allows unequal distribution of BW<sub>t</sub> among the components. This setup permits higher BW<sub>a</sub> to components with larger values of  $\|R_i \phi\|_2^2$ , i.e., signal energy in the high-pass region. Figure 1 shows an example where there is a discrepancy in frequency contents of  $v_x, v_y,$  and  $v_z,$  with  $v_y$ —due to its narrower temporal footprint and higher amplitude—having higher energy in the high-pass region. The DiR method reduces the temporal resolution of  $v_y$ , while assigning excessively large BW<sub>a</sub> to  $v_x$  and  $v_z$ , which is manifested in the form of oscillations. Figure 2 shows that

DiRa exhibits smaller bias and variation in the estimation of peak-velocity. The preliminary results presented in Figure 3 indicate that DiRa is in strong agreement with reference standard. In future we will quantitatively compare DiR and DiRa with the reference standard in vivo.

**Conclusions:** We have presented and validated a new data processing method that improves the reconstruction quality of PC-MRI in terms of artifacts and temporal resolution. This same approach may also be applicable to 7D flow, and other phase-based measurements of dynamic processes, such as DENSE and elastography.

**References:** [1] Pelc et al. J. Magn. Reson. Imag. 1991; 1: 405-413. [2] Ahmad et al. ISMRM 2013; 1336. [3] Breuer et al. Megan. Reson. Med. 2005; 53: 981-985.

$$\text{s.t. } \frac{1}{\lambda_b} + \frac{1}{\lambda_x} + \frac{1}{\lambda_y} + \frac{1}{\lambda_z} = \text{constant} \quad (\text{Eq. 2})$$

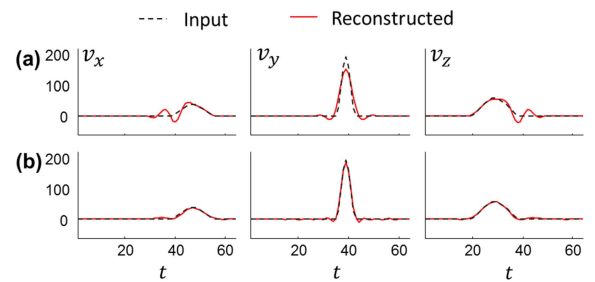


**Figure 1:** Representative simulation results. The true temporal profiles for the three velocity components ( $v_x, v_y, v_z$ ) are shown in dashed black line, and the reconstructed profiles are shown in solid red line. Profile for the background phase ( $v_b$ ) is not shown. (a) Recently proposed DiR method (Eq. 1). (b) The proposed adaptive implementation, DiRa (Eq. 2).

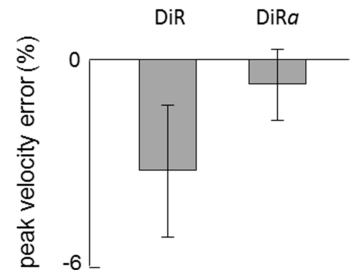


**Figure 2:** Simulation results for peak velocity error. Peak velocities of the two methods were compared for 256 trial runs, each with a different realization of  $v_b, v_x, v_y, v_z$  profiles. One such realization is shown in Figure 1.